

## Electronic structure of short-period $n$ - $p$ GaAs doping superlattices

Kent D. Choquette

*AT&T Bell Laboratories, 600 Mountain Avenue, Murray Hill, New Jersey 07974*

D. K. Misemer

*Photonics Research Laboratory and Science Research Laboratory, 3M Company, St. Paul, Minnesota 55144*

Leon McCaughan

*Electrical and Computer Engineering Department, University of Wisconsin, Madison, Wisconsin 53706*

(Received 20 September 1990; revised manuscript received 3 December 1990)

We present the electronic structure of compensated, noncompensated, and nonequilibrium uniformly doped short-period GaAs doping superlattices. Self-consistent calculations are described, which include miniband dispersion, and can be applied to arbitrarily shaped superlattice potentials. For  $n$ - $p$  superlattices with periods less than 200 Å, we find significant dispersion in the first conduction subband and weak confinement of electrons to the donor layers. Band filling is shown to be the major contribution to the tunability of the electronic structure in these superlattices under excitation, while for periods greater than 200 Å, carrier screening of the superlattice potential dominates the variation. The calculated carrier-recombination lifetimes in short-period doping superlattices are comparable to bulk GaAs.

### I. INTRODUCTION

Doping (also known as  $n$ - $i$ - $p$ - $i$ ) semiconductor superlattices are composed of a periodic sequence of  $n$ - and  $p$ -type impurity layers, possibly with intrinsic regions between, in an otherwise homogeneous semiconductor. They possess a space-charge-induced one-dimensional periodic potential, which creates wells for electrons and holes that are offset by one half period. The attributes of doping superlattices fall between two extremes, depending upon the degree of wave-function coupling through the superlattice barrier between adjacent wells. For long-period doping superlattices<sup>1</sup> with inherently high and wide potential barriers, significant confinement of charge carriers to the doped layers occurs, giving rise to nondispersive energy sublevels in the direction of growth. By contrast, the wave functions in ideal short-period doping superlattices<sup>2</sup> extend into the barrier regions as a consequence of greater tunneling; thus in this regime there is miniband dispersion and significant overlap between electron and hole wave functions.

The electronic structure, i.e., the superlattice potential profile, subband energies, wave functions, carrier distribution, and Fermi energy is dependent upon the density of free carriers for doping superlattices in the ground state. Likewise electrical or optical injection of charge carriers into these materials will have an effect on the nonequilibrium electronic structure. The presence of excess carriers increases the Fermi energy and reduces the superlattice potential by screening the ionized impurities. Knowledge of the electronic structure for the conditions of compensated (depleted ground state), noncompensated (free carriers in ground state), or nonequilibrium (free carriers due to excitation) is crucial in understanding the tunable properties of doping superlattices.

Early research,<sup>1</sup> including electronic-structure calculations,<sup>3-5</sup> has concentrated on uniformly doped GaAs structures with period lengths greater than 500 Å. Shorter-period  $\delta$ -doped  $n$ - $i$ - $p$ - $i$  superlattices have been studied,<sup>2</sup> and energy-band calculations of short-period uniformly doped compensated  $n$ - $i$ - $p$ - $i$  structures have been published.<sup>6,7</sup> Recently we have investigated the optical properties of short-period  $n$ - $p$  doping superlattices.<sup>8,9</sup> In this paper we present detailed calculations of the electronic structure of ideal  $n$ - $p$  GaAs superlattices with period lengths less than 300 Å for compensated, noncompensated, and nonequilibrium conditions. We describe in Sec. II the doping superlattice model and our self-consistent calculations, which take into account miniband dispersion and contain no assumptions on the shape or symmetry of the superlattice potential. The characteristics of long- and short-period doping superlattices are presented and discussed in Sec. III.

### II. DOPING SUPERLATTICE MODEL AND THEORY

Figure 1 shows the band diagram of a long- and short-period  $n$ - $p$  doping superlattice. In our model we assume an ideal superlattice consisting of a periodic and uniform distribution of impurities within the doped layers. The charge of the ionized dopants is considered to be homogeneously smeared out in their respective layers. We therefore omit two aspects:<sup>4</sup> (i) fluctuations in the superlattice potential that would arise from a random spatial distribution of impurities, and (ii) the point-charge character of the dopants, which could lead to bound impurity states or impurity energy bands. Noting this caveat here, the pragmatic significance of the first point is discussed in Sec. III, while the latter aspect is important in the treat-

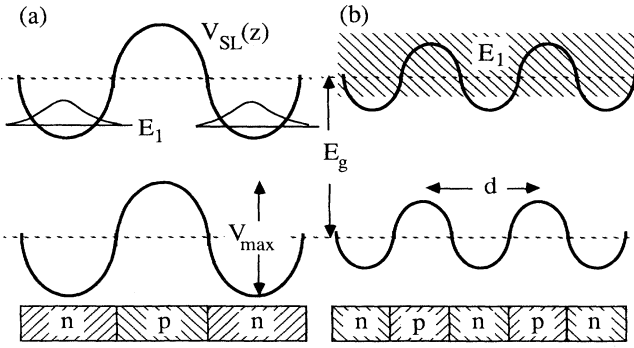


FIG. 1. Real-space band diagram and dopant layer sequence of *n-p* doping superlattices. (a) Long-period superlattice with first electronic energy level and wave function; (b) short-period superlattice with first conduction subband denoted by the hatched area.

ment of excess electrons and holes.

Will free carriers occupy superlattice subband states or impurity states in uniformly doped GaAs doping superlattices? Using similar arguments as given in Ref. 4, we consider a simple cubic array of impurities with concentration  $n_i$ , nearest-neighbor distance  $l_i = 2(4\pi n_i/3)^{-1/3}$ , and associated Bohr radius  $a_i$ . A tight-binding (TB) model corresponding to impurity-bound carriers would be appropriate when  $l_i \gg 2a_i$ , or

$$n_i \ll \frac{3}{4\pi a_i^3}. \quad (1)$$

The opposite extreme is the nearly-free-electron (NFE) model in which the charge carriers are only slightly perturbed by the periodic potential of the ionized dopants and hence will populate subband states. The NFE model will be relevant when the carrier kinetic energy at the Brillouin-zone boundary,  $\hbar^2 \pi^2 / 2m^* l_i^2$ , is greater than the Fourier component of the impurity array potential,  $e^2 / \epsilon l_i$ , where  $m^*$  is the effective mass,  $e$  is the electronic charge, and  $\epsilon$  is the dielectric constant. The NFE criterion is then

$$n_i \gg \frac{48(m^*)^3 e^6}{\hbar^6 \pi^7 \epsilon^3}. \quad (2)$$

Table I shows the criteria limits for silicon donors and beryllium acceptors in GaAs. Since impurity concentrations typically range from  $10^{17}$  to  $10^{19} \text{ cm}^{-3}$ , we see that

TABLE I. The criteria limits for the tight-binding (TB) and nearly-free-electron (NFE) models for Si and Be impurities in GaAs.

Carrier	TB	NFE
Electrons	$n_D \ll 10^{17} \text{ cm}^{-3}$	$n_D \gg 10^{16} \text{ cm}^{-3}$
Heavy holes	$n_A \ll 10^{20}$	$n_A \gg 10^{19}$

the NFE model is applicable for conduction electrons, while the TB model is appropriate for heavy holes in GaAs doping superlattices. Therefore donor impurity states are neglected in our model, whereas excess holes are expected to populate acceptor impurity states above the superlattice modulation of the valence band.

### A. Compensated doping superlattices

Compensated doping superlattices have an equal number of donors and acceptors in each period ( $n_D d_n = n_A d_p$ ). In this simplest case, the compensated superlattice potential profile  $V_{SL}(z)$  is dependent only upon the fabrication parameters: donor concentration  $n_D$  with layer thickness  $d_n$  and acceptor concentration  $n_A$  with layer thickness  $d_p$ . The depletion widths of the individual *p-n* junctions are greater than the dopant layer thicknesses for the superlattices considered here. Thus in the ground state (no carrier injection) the superlattice potential arises from only the ionized impurities and can be determined analytically from Poisson's equation. The amplitude of the compensated superlattice potential modulation will be

$$V_{\max} = \frac{e^2}{\epsilon} \left[ n_D \left( \frac{d_n}{2} \right)^2 + n_A \left( \frac{d_p}{2} \right)^2 \right]. \quad (3)$$

Notice that through judicious selection of the superlattice fabrication parameters a continuous variation of potential amplitude and periodicity can be independently achieved. However, for thin dopant layers, large impurity concentrations are necessary to maintain a meaningful superlattice potential amplitude,<sup>8</sup> and thus short-period doping superlattices require highly doped layers.

It has been well established for semiconductor superlattices that charge carriers near the band edges behave as free carriers with an effective mass determined by the bulk band curvature in the directions parallel to the superlattice layers, but are strongly perturbed in the direction of superlattice growth. Using the effective-mass approximation, the energy-band structure of the superlattice is given by

$$E(k_z, k_t) = E_i(k_z) + \frac{\hbar^2 k_t^2}{2m^*}, \quad (4)$$

where  $E_i$  is the subband energy ( $i$  is the subband index) and  $k_z$  and  $k_t$  are the wave vectors perpendicular and parallel, respectively, to the superlattice layers ( $z$  is the direction of superlattice growth). We use the envelope-function approximation to separate the wave functions into bulk and superlattice components, and thus the subband energies and wave functions  $\Psi_{ik_z}$  can be determined from the one-dimensional Schrödinger equation:

$$\frac{\hbar^2}{2m^*} \frac{d^2}{dz^2} \Psi_{ik_z} + [E_i(k_z) - V_{SL}(z)] \Psi_{ik_z} = 0. \quad (5)$$

When the superlattice potential modulation is large and the band index is small, the energy subbands will have no

$k_z$  dependence; however, for short-period structures even the lowest-energy subband will exhibit dispersion.<sup>6,8</sup>

To solve Eq. (5) at an arbitrary point in the superlattice mini-Brillouin zone, we utilize a procedure similar to that described by Zeller *et al.*,<sup>3</sup> but without assumptions concerning the symmetry<sup>3,4</sup> or shape<sup>6,7</sup> of the potential, nor demands for parabolic bands, as other methods require. Given the superlattice period length  $d$ , we choose two functions  $\psi_L^1$  and  $\psi_L^2$  defined on the left half of the superlattice unit cell by the initial conditions

$$\psi_L^1 \left[ \frac{-d}{2} \right] = 1, \quad \frac{d}{dz} \psi_L^1 \left[ \frac{-d}{2} \right] = 0, \quad (6a)$$

$$\psi_L^2 \left[ \frac{-d}{2} \right] = 0, \quad \frac{d}{dz} \psi_L^2 \left[ \frac{-d}{2} \right] = 1. \quad (6b)$$

Similarly we choose two functions  $\psi_R^1$  and  $\psi_R^2$  defined on the right half of the unit cell by the initial conditions

$$\psi_R^1 \left[ \frac{d}{2} \right] = 1, \quad \frac{d}{dz} \psi_R^1 \left[ \frac{d}{2} \right] = 0, \quad (7a)$$

$$\psi_R^2 \left[ \frac{d}{2} \right] = 0, \quad \frac{d}{dz} \psi_R^2 \left[ \frac{d}{2} \right] = 1. \quad (7b)$$

The functions  $\psi^1$  and  $\psi^2$  are independent solutions of Eq. (5), and can be integrated to the center of the unit cell by standard numerical techniques.

A general solution of the Schrödinger equation may be written as

$$\psi(z) = \alpha \psi^1(z) + \beta \psi^2(z), \quad (8)$$

where  $\alpha$  and  $\beta$  are arbitrary complex constants. Matching the wave function and its first derivative at the center of the unit cell yields

$$\mathbf{M}_L \begin{bmatrix} \alpha_L \\ \beta_L \end{bmatrix} = \mathbf{M}_R \begin{bmatrix} \alpha_R \\ \beta_R \end{bmatrix}, \quad (9)$$

where

$$\mathbf{M}_{L,R} = \begin{bmatrix} \psi_{L,R}^1(0) & \psi_{L,R}^2(0) \\ \frac{d}{dz} \psi_{L,R}^1(0) & \frac{d}{dz} \psi_{L,R}^2(0) \end{bmatrix}. \quad (10)$$

It can be easily shown that  $\det \mathbf{M}_{L,R} = 1$ . Thus Eq. (9) may be rewritten as

$$\begin{bmatrix} \alpha_R \\ \beta_R \end{bmatrix} = \mathbf{M}_R^{-1} \mathbf{M}_L \begin{bmatrix} \alpha_L \\ \beta_L \end{bmatrix} = \mathbf{W} \begin{bmatrix} \alpha_L \\ \beta_L \end{bmatrix}. \quad (11)$$

Using Bloch's theorem we know that

$$\psi \left[ \frac{d}{2} \right] = e^{ikd} \psi \left[ \frac{-d}{2} \right], \quad (12a)$$

$$\frac{d}{dz} \psi \left[ \frac{d}{2} \right] = e^{ikd} \frac{d}{dz} \psi \left[ \frac{-d}{2} \right], \quad (12b)$$

from which follows

$$\alpha_R = e^{ikd} \alpha_L, \quad (13a)$$

$$\beta_R = e^{ikd} \beta_L. \quad (13b)$$

Using Eqs. (11), (13a), and (13b), we evaluate the eigenvalue condition to be

$$\begin{bmatrix} e^{ikd} & 0 \\ 0 & e^{ikd} \end{bmatrix} \begin{bmatrix} \alpha_L \\ \beta_L \end{bmatrix} = \mathbf{W} \begin{bmatrix} \alpha_L \\ \beta_L \end{bmatrix}, \quad (14)$$

which leads to the eigenvalue equation

$$\text{Tr}[\mathbf{W}] - \cos(kd) = 0. \quad (15)$$

This method of solving the Schrödinger equation can be applied to any arbitrary one-dimensional periodic potential and thus is applicable to other problems, for example nonsymmetric quantum wells or compositional superlattices with modulation doping.

### B. Noncompensated doping superlattices

For noncompensated doping superlattices ( $n_D d_n \neq n_A d_p$ ), the superlattice potential arises from both ionized impurities and excess free carriers. For  $n$ -type noncompensated superlattices,<sup>8</sup> the one-dimensional superlattice potential is

$$\begin{aligned} V_{\text{SL}}(z) = & \frac{e^2}{\epsilon} \int_0^z dz' \int_0^{z'} [n_A(z'') - n_D(z'')] dz'' \\ & + \frac{e^2}{\epsilon} \int_0^z dz' \int_0^{z'} n_e(z'') dz'' \\ & - 0.611 \frac{e^2}{\epsilon} \left[ \frac{3n_e(z)}{4\pi} \right]^{1/3}. \end{aligned} \quad (16)$$

The last term is the local exchange potential,<sup>10</sup> where  $n_e$  is the free-electron density. Since electrons populate superlattice subband states, the electronic distribution is given by

$$n_e(z) = \sum_i \frac{m^*}{\pi^2 \hbar^2} \int_0^{\pi/d} |\psi_{ik_z}|^2 dk_z \int_0^\infty f[E_i + E_i(k_z)] dE_i, \quad (17)$$

where  $f[E]$  is the Fermi-Dirac distribution. The Fermi energy  $E_F$  is found from satisfying the condition

$$n_e = \sum_i \frac{m^*}{\pi^2 \hbar^2} \int_0^{\pi/d} dk_z \int_0^\infty f[E_i + E_i(k_z)] dE_i, \quad (18)$$

where

$$n_e = \frac{n_D d_n - n_A d_p}{d}. \quad (19)$$

The electronic structure of  $n$ -type noncompensated superlattices is found by numerically solving Eqs. (5) and (16)–(18) utilizing an iterative self-consistent scheme. For  $p$ -type noncompensated doping superlattices, a space-charge model to account for the effect of excess holes is utilized, as discussed in the following section.

### C. Nonequilibrium doping superlattices

The preceding sections have considered doping superlattices in the absence of carrier injection. The excited-

state electronic structure of a doping superlattice can differ dramatically from the ground state because of long carrier-recombination lifetimes, which arise from the confinement of nonequilibrium electrons (holes) in the *n* layers (*p* layers) and from the spatial separation of the carriers. Thus with weak optical or electrical carrier injection, excess carrier densities can be maintained, which screen the ionized impurities, reducing the space-charge potential, and lead to a variation in the superlattice electronic structure.<sup>1</sup>

For excited compensated superlattices the electron and hole densities  $n_e$  and  $n_h$ , respectively, are the nonequilibrium concentrations. Noncompensated excited superlattices will have a contribution to the free charge from the dominant impurity as well as from carrier injection. The self-consistent calculation of the superlattice potential profile, conduction subband states, the electronic distribution, and the electron quasi-Fermi-energy follow as described in the preceding section, only now the contribution of holes must also be included. We have shown that holes will populate impurity states rather than valence superlattice states; due to the confining superlattice potential we assume that the filled acceptor states lie within the central region of the *p* layers.<sup>4</sup> Excess holes then create a neutral region within the acceptor layers of width

$$l_h = \frac{n_h^{(2)}}{n_A} = \frac{n_h d}{n_A}, \quad (20)$$

where  $n_h^{(2)}$  is the areal hole concentration per superlattice period. (Note the hole quasi-Fermi-level is pinned at the acceptor impurity-state energy.) Therefore excess holes are included in the self-consistent calculation by simply neutralizing a portion of the ionized acceptor charge in the determination of the superlattice potential,  $V_{SL}(z)$ .

To conclude this section, we derive an expression for the carrier-recombination lifetime in nonequilibrium doping superlattices. Observe that within our model the hole density is 0 or  $n_h(z) \gg n_e(z)$ , which allows us to write the recombination rate in terms of the minority carrier.<sup>11</sup> Thus within the hole accumulation region,

$$\frac{dn_e(z)}{dt} = -\frac{n_e(z)}{\tau_{\text{bulk}}}, \quad (21)$$

where  $\tau_{\text{bulk}}$  is the bulk radiative recombination lifetime and nonradiative transitions are neglected. The effective recombination rate for areal charge density is then given by

$$\frac{dn_e^{(2)}}{dt} = \int_0^{l_h} \frac{dn_e(z)}{dt} dz = \frac{-1}{\tau_{\text{bulk}}} \int_0^{l_h} n_e(z) dz. \quad (22)$$

In analogy with Eq. (21), we define an effective recombination lifetime,  $\tau_{\text{eff}}$ , for the areal charge density,

$$\frac{dn_e^{(2)}}{dt} = -\frac{n_e^{(2)}}{\tau_{\text{eff}}}, \quad (23)$$

and conclude

$$\tau_{\text{eff}} = \tau_{\text{bulk}} \frac{\int_0^d n_e(z) dz}{\int_0^{l_h} n_e(z) dz} = \frac{\tau_{\text{bulk}} n_e d}{\int_0^{l_h} n_e(z) dz}. \quad (24)$$

It can be seen from Eq. (24) that the effective recombination lifetime scales inversely with the fraction of the nonequilibrium electron density within the hole accumulation region in the acceptor layer. Notice no explicit assumption concerning the recombination mechanism has been made, rather we assume only that the same recombination processes apply to both the bulk semiconductor and the doping superlattice.

### III. RESULTS AND DISCUSSION

In Fig. 2 we show the ground-state conduction-band electronic structure versus period length for compensated *n-p* GaAs superlattices with equal impurity layer thicknesses. In this and the following figures the zero of energy is the bottom of the conduction potential well, which is  $V_{\text{max}}/2$  below the bulk GaAs band edge. The superlattice potential amplitude increases quadratically with layer thickness, as expected from Eq. (3), and the lowest sublevel becomes dispersive at a period length of 200 Å. Either subband states or miniband gaps can be engineered to coincide with the top of the potential well depending on the fabrication parameters.

Figure 3(a) depicts the ground-state electronic structure versus period length for *n*-type noncompensated superlattices with equal dopant layer thicknesses and an excess electron density of  $n_e = 7.5 \times 10^{17} \text{ cm}^{-3}$ . Similar trends as seen in Fig. 2 also hold, only now the potential modulation increases less with period length due to screening of the ionized impurities by the free electrons. Notice that for this particular carrier density the Fermi energy lies above the space-charge potential for periods less than 160 Å. In Fig. 3(b) we plot the electronic distribution across a period for *n*-type superlattices with periods of 250, 150, and 120 Å. The superlattice with the

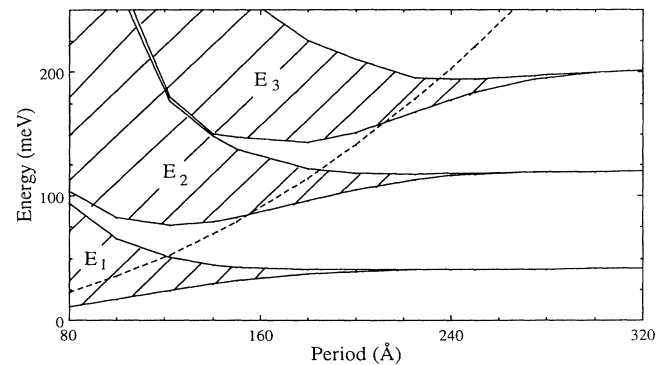


FIG. 2. Ground-state electronic structure of compensated GaAs doping superlattices with  $n_D = n_A = 4 \times 10^{18} \text{ cm}^{-3}$  and  $d_n = d_p = \frac{1}{2}d$ . The hatched areas represent dispersive subbands and the dashed curve is the superlattice potential magnitude  $V_{\text{max}}$ .

longest period exhibits strong confinement of the electrons to the donor layer—the exponential decay of the carrier distribution into the acceptor layer implies long recombination lifetimes, as we will see below. The shorter-period superlattices show less confinement, which is consistent with the formation of dispersive subbands and shorter recombination lifetimes.

Tunability of the electronic structure of nonequilibrium compensated GaAs doping superlattices is shown in Fig. 4. We point out several differences between the characteristics of doping superlattices with periods of 300 and 120 Å. First, notice that the potential magnitude of the 300-Å-period structure changes more rapidly with the carrier density than the shorter-period superlattice. Hence screening of the space-charge potential dominates the variation of the electronic structure for long-period superlattices, while band filling (the shift of the electron quasi-Fermi-level) is relatively more important in short-period superlattices. The optical band gap corresponds to the difference in the quasi-Fermi-energies of electrons and holes.<sup>1</sup> Tunability of the band gap then arises from changing the potential modulation and shifting the quasi-Fermi-energies. Therefore, a variable optical band

gap in long-period superlattices arises predominantly from carrier confinement and space-charge screening, while in short-period superlattices band filling is the major contribution.

A second observation is that the 120-Å-period superlattice can accommodate more electrons in a given subband than the 300-Å-period superlattice. The first subband is occupied in Fig. 4(b) at  $n_e \approx 4 \times 10^{17} \text{ cm}^{-3}$ , while the first energy level in Fig. 4(a) is filled at a much smaller carrier level. This is because the shorter-period superlattice has a larger first mini-Brillouin-zone and incorporates a greater number of states in  $k$  space than a longer-period superlattice.<sup>8</sup> Finally, notice the change in the slope of the electron quasi-Fermi-level when it passes through a miniband; this arises from the abrupt change in the density of states. This change of slope is less apparent when the quasi-Fermi-energy passes through a dispersive miniband since the change in the density of states for a dispersive miniband is more gradual.<sup>7</sup>

Using Eq. (24) we plot in Fig. 5 the effective recombination lifetime versus nonequilibrium carrier density for the doping superlattices portrayed in Fig. 4. The bulk GaAs recombination lifetime is taken to be 1 nsec. The

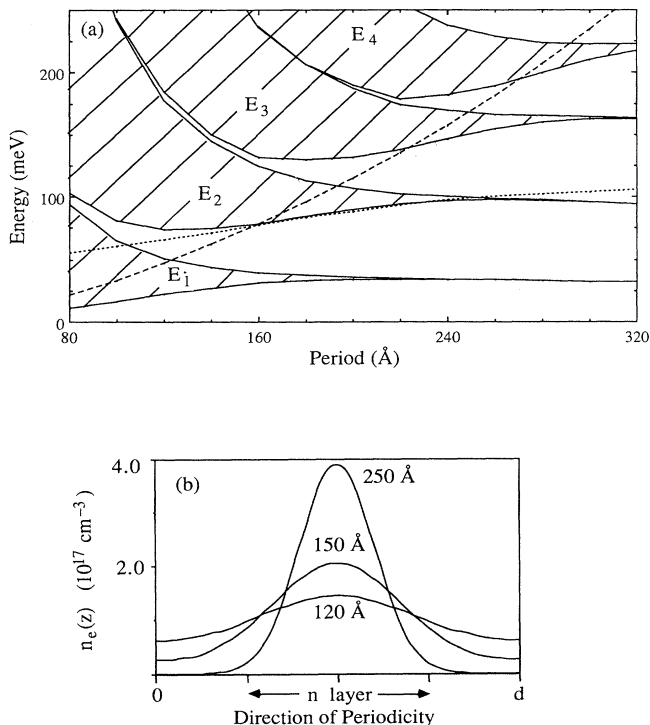


FIG. 3. (a) Ground-state electronic structure of noncompensated GaAs doping superlattices with  $n_D = 4.5 \times 10^{18} \text{ cm}^{-3}$ ,  $n_A = 3 \times 10^{18} \text{ cm}^{-3}$ , and  $d_n = d_p = \frac{1}{2}d$ . The hatched areas represent dispersive subbands, the dashed curve is  $V_{\text{max}}$ , and the dotted curve is the Fermi level. (b) Ground-state electronic distribution for  $n$ -type noncompensated superlattices of (a) with periods of 250, 150, and 120 Å.

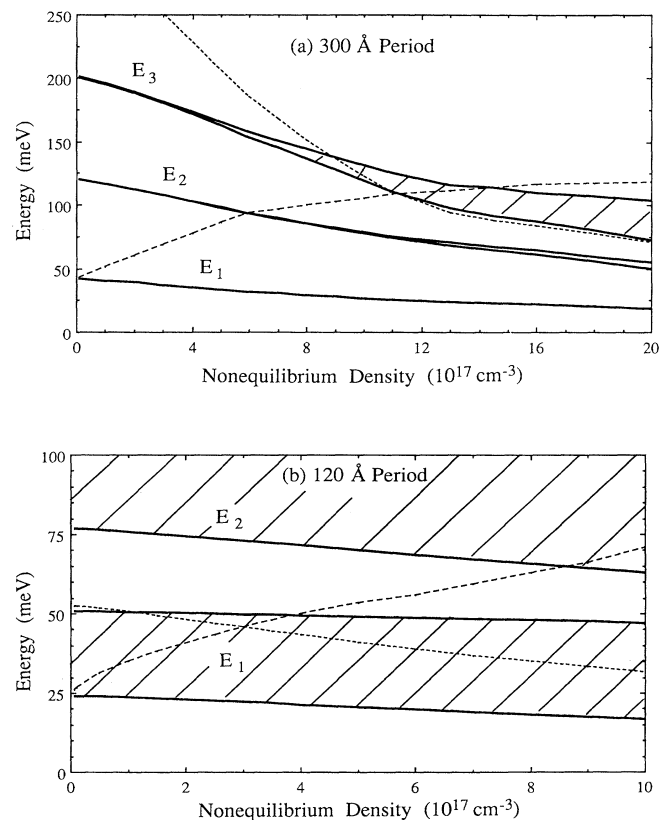


FIG. 4. Excited-state electronic structure of compensated GaAs doping superlattices with  $n_D = n_A = 4 \times 10^{18} \text{ cm}^{-3}$  and  $d_n = d_p = \frac{1}{2}d$ . The hatched areas represent dispersive subbands, the dashed curves are  $V_{\text{max}}$ , and the dotted curves are the electron quasi-Fermi-energies. (a)  $d = 300 \text{ Å}$ ; (b)  $d = 120 \text{ Å}$ .

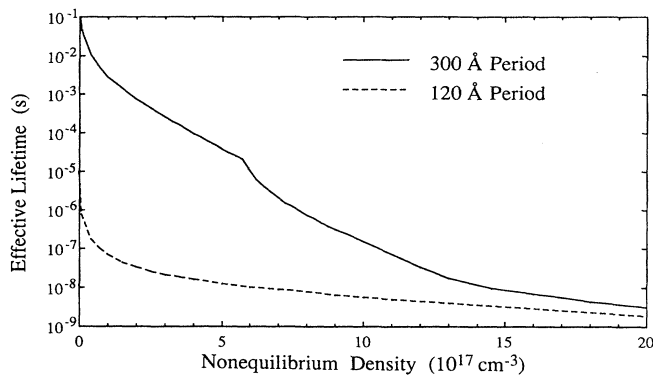


FIG. 5. Effective recombination lifetime for excited-state GaAs doping superlattices with  $n_D = n_A = 4 \times 10^{18} \text{ cm}^{-3}$ ,  $d_n = d_p = \frac{1}{2}d$ , and period lengths of 120 and 300 Å.

slope discontinuity observed for the 300-Å-period superlattice at  $n_e \approx 6 \times 10^{17} \text{ cm}^{-3}$  occurs when the electron quasi-Fermi-energy rises through the second energy sublevel. Notice that at low injection densities the recombination lifetimes of the two superlattices differ by many orders of magnitude. The short-period superlattice lifetime approaches to within a factor of 10 the bulk lifetime for carrier densities greater than  $6 \times 10^{17} \text{ cm}^{-3}$ . This occurs at a much lower carrier concentration than for the longer-period superlattice because of less carrier confinement [e.g., see Fig. 3(b)] and therefore greater overlap between electron and hole wave functions in the shorter-period structure. When the effective recombina-

tion lifetime becomes comparable to the bulk lifetime, excess carrier densities and tunability of the electronic structure will not persist. In fact,  $\delta$ -doped *n-i-p-i* GaAs superlattices with sufficiently small period lengths exhibit stable optical band gaps.<sup>2</sup>

The electronic-structure calculations presented herein have assumed an ideal doping distribution within the superlattice layers. A random arrangement of impurities will give rise to random potential fluctuations in the space-charge potential.<sup>4</sup> A growth technique such as migration-enhanced molecular-beam epitaxy<sup>12</sup> coupled with a correlated dopant distribution predicted<sup>13</sup> for highly doped layers might accomplish a greater degree of ordering of the impurities in uniformly doped layers. It has also been shown that  $\delta$ -doped *n-i-p-i* superlattices exhibit reduced random potential fluctuations,<sup>14</sup> and thus our findings are also applicable to these doping superlattice materials.

In conclusion, we have outlined a self-consistent scheme to determine the space-charge potential profile, subband energies, wave functions, carrier distribution, and Fermi energy of ideal short-period doping superlattices. The results of compensated, noncompensated, and nonequilibrium cases are shown for uniformly doped *n-p* GaAs superlattices with periods less than 300 Å. We find significant dispersion in the first conduction subband for periods less than 200 Å and weak confinement of electrons to the donor layers, which results in carrier-recombination lifetimes comparable to bulk GaAs. For these short-period superlattices we determine that band filling effects dominate confined carrier screening of the superlattice potential, both of which lead to tunable properties in semiconductor doping superlattices.

<sup>1</sup>For a review of long-period doping superlattices, see G. H. Dohler and K. Ploog, in *Synthetic Modulated Structures*, edited by L. Chang and B. Giessen (Academic, New York, 1985).

<sup>2</sup>E. F. Schubert, Y. Horikoshi, and K. Ploog, *Phys. Rev. B* **32**, 1085 (1985); E. F. Schubert, J. E. Cunningham, and W. T. Tsang, *ibid.* **36**, 1348 (1987).

<sup>3</sup>Ch. Zeller, B. Vinter, and G. Abstreiter, *Phys. Rev. B* **26**, 2124 (1982).

<sup>4</sup>P. Ruden and G. H. Dohler, *Phys. Rev. B* **27**, 3538 (1983).

<sup>5</sup>S. Brand and R. A. Abram, *J. Phys. C* **16**, 6111 (1983).

<sup>6</sup>H. Yan and H. X. Jiang, *Phys. Rev. B* **37**, 6425 (1988).

<sup>7</sup>J. Y. Lin and H. X. Jiang, *Phys. Rev. B* **40**, 5561 (1989).

<sup>8</sup>K. D. Choquette, L. McCaughan, and D. K. Misemer, *J. Appl.*

*Phys.* **66**, 4387 (1989).

<sup>9</sup>K. D. Choquette, L. McCaughan, D. K. Misemer, J. E. Potts, and G. D. Verstrom (unpublished).

<sup>10</sup>W. Kohn and L. J. Sham, *Phys. Rev.* **140**, A1133 (1965).

<sup>11</sup>S. M. Sze, *Physics of Semiconductor Devices*, 2nd ed. (Wiley, New York, 1981), p. 37.

<sup>12</sup>Y. Horikoshi, M. Kawashima, and Y. Yamaguchi, *Jpn. J. Appl. Phys.* **27**, 169 (1988).

<sup>13</sup>E. F. Schubert, J. M. Kuo, R. F. Kopt, H. S. Luftman, L. C. Hopkins, and N. J. Sauer, *J. Appl. Phys.* **67**, 1969 (1990).

<sup>14</sup>E. F. Schubert, T. D. Harris, and J. E. Cunningham, *Appl. Phys. Lett.* **53**, 2208 (1988).